

Optimal Control of a Beam with Discontinuously Distributed Piezoelectric Sensors and Actuators

Feng Chen, Ming Hong, Meiting Song* and Hongyu Cui

School of Naval Architecture Engineering, Dalian University of Technology, Dalian 116024, China

Abstract: Because of its light weight, broadband, and adaptable properties, smart material has been widely applied in the active vibration control (AVC) of flexible structures. Based on a first-order shear deformation theory, by coupling the electrical and mechanical operation, a 4-node quadrilateral piezoelectric composite element with 24 degrees of freedom for generalized displacements and one electrical potential degree of freedom per piezoelectric layer was derived. Dynamic characteristics of a beam with discontinuously distributed piezoelectric sensors and actuators were presented. A linear quadratic regulator (LQR) feedback controller was designed to suppress the vibration of the beam in the state space using the high precise direct (HPD) integration method.

Keywords: smart material; first-order shear deformation; high precise direct (HPD); linear quadratic regulator (LQR); beam; piezoelectric sensor; piezoelectric actuator

Article ID: 1671-9433(2012)01-0044-08

1 Introduction

Piezoceramics, known for their light weight, broadband, and adaptable qualities, have the potential to be applied widely in the active vibration control (AVC) of ship structures. Many studies have already been carried out on this topic. Investigation on the AVC characteristics of piezoelectric composite structures was shown to improve the structural technical reserves of ships (Song *et al.*, 2006). Analytic and experimental development of piezoelectric actuators as elements of intelligent structures were presented (Crawley and de Luis, 1986), with the analytic models for segmented piezoelectric actuators being bonded to an elastic substructure or embedded in a laminated composite. A finite element model with potential degrees of freedom was proposed, and the dynamic characteristics of a plate with distributed piezoelectric sensors and actuators were simulated (Tzou *et al.*, 1990). Theoretical solution of the dynamic equation of a simply supported rectangular plate was discussed, and the properties of sensors and actuators were given (Ray *et al.*, 1993). An 8-node quadrilateral isoparametric element, with a laminate plate being governed by distributed piezoelectric sensors and actuators, was put forward based on a negative velocity feedback control method (Samanta *et al.*, 1996). Nonlinear dynamic responses of smart structures were analyzed, and a 20-node body element with potential degrees of freedom was used to develop the model (Sung *et al.*, 2000). Vibrations of a cantilever under transient or harmonic excitations were

controlled (Simoes-Moita, 2004), using a nonconforming single layer triangular plate/shell element based on the Kirchhoff classical laminated theory and a negative velocity feedback control theory. The affection of temperature in the governing equation was considered (Narayanan *et al.*, 2003), and positive velocity feedback control, Lyapunov feedback control, and LQR control theories were compared while structures were subjected to a transient or harmonic excitation. A 2-node piezothermoelastic composite element with distributed piezoelectric sensor and actuator layers was discussed based on a high-order displacement field, a new high-order electrical potential field, and a linear temperature field. Vibrations of a beam were suppressed using a constant-gain feedback control theory (Jiang *et al.*, 2007). AVC of piezoelectric flexible structures was investigated by assuming the transversal distribution of the potential—a combination of a half-cosine and linear distribution (Pietrzakowski, 2008).

In this paper, a 4-node quadrilateral isoparametric element is presented to simulate a shell element with distributed piezoelectric sensors and actuators. Six generalized displacement degrees of freedom per node and one electrical potential degree of freedom per piezoelectric layer are considered. The governing equation, being derived on the basis of the Midlin first-order shear deformation theory and Hamilton's principle, is solved by a high precise direct (HPD) integration method in a state space, and the LQR method is also applied to design an output feedback controller. AVC of a piezoelectric composite cantilever is simulated through the corresponding FORTRAN finite element programs. Furthermore, in this paper, modeling development is based on a linear approach.

Received date: 2011-06-20.

Foundation item: Supported by the National Natural Science Foundation of China (51079027).

***Corresponding author Email:** smt19870105@163.com

© Harbin Engineering University and Springer-Verlag Berlin Heidelberg 2012

2 A finite element model for piezoelectric composite structures

2.1 Basic assumption

A shell element, on which the distributed piezoelectric sensor and actuator are bounded, is shown in Fig.1. Each layer of the composite element is homogeneous, transversely isotropic (the host structure is isotropic), and linearly elastic. The poling direction of the piezoelectric layers coincides with the z -axis, and a linear function is used to describe the potential distribution along the thickness direction. Additionally, bonding between piezoelectric layers and the host structure is considered to be perfect; in other words, the bonding layers are negligible.

2.2 Displacement fields

The displacement components of a generic point in the piezoelectric composite element local axes (x, y, z) are assumed to be

$$\begin{cases} u(x, y, z, t) = u_0(x, y, t) + z\theta_y \\ v(x, y, z, t) = v_0(x, y, t) - z\theta_x \\ w(x, y, z, t) = w_0(x, y, t) \end{cases} \quad (1)$$

where u_0 , v_0 , and w_0 are the displacements of the point on the neutral surface in the x , y , and z directions, respectively; θ_x and θ_y are the rotations of the x and y axes, respectively.

2.3 Strain-displacement relationship

The strain-displacement relationships for elements based on the Mindlin first-order shear deformation theory have the form

$$\begin{Bmatrix} \epsilon_x^M \\ \epsilon_y^M \\ \gamma_{xy}^M \\ \epsilon_x^B \\ \epsilon_y^B \\ \gamma_{xy}^B \\ \gamma_{yz} \\ \gamma_{xz} \end{Bmatrix} = \begin{bmatrix} \frac{\partial}{\partial x} & 0 & 0 & 0 & 0 \\ 0 & \frac{\partial}{\partial y} & 0 & 0 & 0 \\ \frac{\partial}{\partial y} & \frac{\partial}{\partial x} & 0 & 0 & 0 \\ 0 & 0 & 0 & 0 & z\frac{\partial}{\partial x} \\ 0 & 0 & 0 & -z\frac{\partial}{\partial y} & 0 \\ 0 & 0 & 0 & -z\frac{\partial}{\partial x} & z\frac{\partial}{\partial y} \\ 0 & 0 & \frac{\partial}{\partial y} & -1 & 0 \\ 0 & 0 & \frac{\partial}{\partial x} & 0 & 1 \end{bmatrix} \begin{Bmatrix} u_0 \\ v_0 \\ \theta_x \\ \theta_y \end{Bmatrix} \quad (2)$$

It can be further expressed as

$$\epsilon = B^{mb} a \quad (3)$$

Then the mechanical strain $\bar{\epsilon}$ of a generic point in the

element is given by

$$\bar{\epsilon} = \epsilon^m + \epsilon^b \quad (4)$$

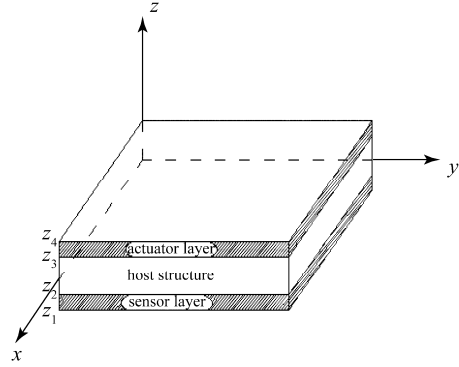


Fig.1 Coordinates of a piezoelectric composite element

2.4 Piezoelectric laminate constitutive equations

The linear piezoelectric constitutive equations coupling the elastic field and the electric field can be expressed as (Tiersten, 1969)

$$\begin{cases} \sigma = Q\epsilon - eE \\ D = e^T \epsilon + PE \end{cases} \quad (5)$$

where σ and ϵ are the stress vector and the strain vector, respectively, Q the symmetric elastic constitutive matrix, e the piezoelectric stress constant matrix, E the electric field vector, D the electric displacement vector, and P is the symmetric dielectric matrix.

The relationship between the electric field and potential is $E = -\nabla\phi$. The electric field is considered as $E = \{0 \ 0 \ -E_z\}^T$, where $E_z = -\phi/t$, and ϕ is the electric potential, which is assumed to be applied and varying linearly in the thickness direction of the piezoelectric layers.

Setting $\hat{\epsilon} = \begin{Bmatrix} \epsilon \\ -E \end{Bmatrix}$ and $\hat{\sigma} = \begin{Bmatrix} \sigma \\ D \end{Bmatrix}$, Eq.(5) takes the form as follows

$$\begin{Bmatrix} \sigma \\ D \end{Bmatrix} = \begin{bmatrix} Q & e \\ e^T & -P \end{bmatrix} \begin{Bmatrix} \epsilon \\ -E \end{Bmatrix} \quad \hat{\sigma} = \hat{C} \hat{\epsilon} \quad (6)$$

The relationship between the electric field and potential can be written as Eq.(7) if several piezoelectric layers are considered.

$$\begin{Bmatrix} E_1 \\ \vdots \\ E_n \end{Bmatrix} = -B^{\phi} \begin{Bmatrix} \phi_1 \\ \vdots \\ \phi_n \end{Bmatrix} \quad (7)$$

where the electric field-potential matrix is $\mathbf{B}^\phi = \begin{bmatrix} 1/t_1 & \cdots & 0 \\ \vdots & \ddots & \vdots \\ 0 & \cdots & 1/t_n \end{bmatrix}$.

2.5 Finite element formulations of a piezoelectric composite structure

The dynamic equations of piezoelectric composite structures can be derived from Hamilton's principle:

$$\int_{t_1}^{t_2} \left[\sum_{k=1}^n \left(\int_A \int_{z_{k-1}}^{z_k} \delta \hat{\mathbf{e}}^\top \hat{\mathbf{C}} \hat{\mathbf{e}} dz dA - \int_A \int_{z_{k-1}}^{z_k} \delta \dot{\mathbf{u}}^\top \rho_k \dot{\mathbf{u}} dz dA \right) - \delta W_{de} \right] dt = 0 \quad (8)$$

where the three terms in the formulation are the strain energy, the virtual kinetic energy, and the virtual external work, respectively. The virtual external work is given by

$$W_{de} = \int_V \mathbf{u}^\top \mathbf{f}_v dV + \int_S \mathbf{u}^\top \mathbf{f}_s dS + \sum_i \mathbf{u}_i^\top \mathbf{f}_{ci} + \int_S \boldsymbol{\phi}^\top \mathbf{q} dS \quad (9)$$

where \mathbf{f}_v the body force, \mathbf{f}_s the surface force, \mathbf{f}_{ci} the concerned force on the i th node, and \mathbf{q} is the surface electric charge.

The finite element selected in this paper is a 4-node and bilinear displacement element with 24 generalized displacement degrees of freedom and one electric degree of freedom per piezoelectric layer. The element local displacements are expressed in terms of nodal variables through the shape function.

$$\mathbf{u} = \mathbf{Z} \left(\sum_{i=1}^4 N_i \mathbf{d}_i \right) = \mathbf{Z} \mathbf{d} \quad (10)$$

$$\text{where } \mathbf{Z} = \begin{bmatrix} 1 & 0 & 0 & 0 & -z \\ 0 & 1 & 0 & z & 0 \\ 0 & 0 & 1 & 0 & 0 \end{bmatrix}, \quad N_i = \frac{1}{4} (1 + \xi \xi_i) (1 + \eta \eta_i),$$

the vector of generalized displacement is

$$\mathbf{d}_i = \{u_{0i} \quad v_{0i} \quad w_{0i} \quad \theta_{xi} \quad \theta_{yi} \quad \phi_i^A \quad \phi_i^S\}^\top$$

Substituting Eq.(3), Eq.(6), Eq.(7), and Eq.(10) into Eq.(8), it becomes

$$\begin{aligned} & \int_{t_1}^{t_2} \left\{ \sum_{k=1}^n \left(\int_A \int_{z_{k-1}}^{z_k} \delta \begin{Bmatrix} \mathbf{a} \\ \boldsymbol{\phi} \end{Bmatrix}^\top \begin{bmatrix} \mathbf{B}^{mb} & \mathbf{0} \\ \mathbf{0} & \mathbf{B}^\phi \end{bmatrix} \begin{bmatrix} \mathbf{Q} & \mathbf{e} \\ \mathbf{e}^\top & -\mathbf{P} \end{bmatrix} \begin{bmatrix} \mathbf{B}^{mb} & \mathbf{0} \\ \mathbf{0} & \mathbf{B}^\phi \end{bmatrix} \begin{Bmatrix} \mathbf{a} \\ \boldsymbol{\phi} \end{Bmatrix} dz dA - \right. \right. \\ & \left. \int_A \int_{z_{k-1}}^{z_k} \delta \begin{Bmatrix} \dot{\mathbf{a}} \\ \dot{\boldsymbol{\phi}} \end{Bmatrix}^\top \mathbf{N}^\top \mathbf{m} \mathbf{N} \begin{Bmatrix} \dot{\mathbf{a}} \\ \dot{\boldsymbol{\phi}} \end{Bmatrix} dz dA \right) + \int_V \delta \mathbf{a}^\top \mathbf{N}^\top \mathbf{f}_v dV + \\ & \left. \int_S \delta \mathbf{a}^\top \mathbf{N}^\top \mathbf{f}_s dS + \delta \mathbf{a}^\top \mathbf{f}_c + \int_S \mathbf{Q} \delta \boldsymbol{\phi} dS \right\} dt = 0 \end{aligned} \quad (11)$$

where $\mathbf{m} = \sum_{k=1}^n \rho_k \int_{z_{k-1}}^{z_k} \mathbf{Z}^\top \mathbf{Z} dz$.

From Eq.(11), the stiffness and mass matrices of the piezoelectric composite element can be written as

$$\mathbf{K} = \begin{bmatrix} \mathbf{K}_{uu} & \mathbf{K}_{u\phi} \\ \mathbf{K}_{\phi u} & \mathbf{K}_{\phi\phi} \end{bmatrix} = \sum_{k=1}^n \int_A \int_{z_{k-1}}^{z_k} \begin{bmatrix} \mathbf{B}^{mb} & \mathbf{0} \\ \mathbf{0} & \mathbf{B}^\phi \end{bmatrix}^\top \begin{bmatrix} \mathbf{Q} & \mathbf{e} \\ \mathbf{e}^\top & -\mathbf{P} \end{bmatrix}_k \begin{bmatrix} \mathbf{B}^{mb} & \mathbf{0} \\ \mathbf{0} & \mathbf{B}^\phi \end{bmatrix} dz dA \quad (12)$$

$$\mathbf{M} = \begin{bmatrix} \mathbf{M}_{uu} & \mathbf{0} \\ \mathbf{0} & \mathbf{0} \end{bmatrix} = \int_A \mathbf{N}^\top \mathbf{m} \mathbf{N} dA = \int_A \mathbf{N}^\top \left(\sum_{k=1}^n \rho_k \int_{z_{k-1}}^{z_k} \mathbf{Z}^\top \mathbf{Z} dz \right) \mathbf{N} dA \quad (13)$$

After local-global transformations, the governing equations of the assembled system are

$$\begin{bmatrix} \mathbf{M}_{uu} & \mathbf{0} \\ \mathbf{0} & \mathbf{0} \end{bmatrix} \begin{Bmatrix} \ddot{\mathbf{d}} \\ \ddot{\boldsymbol{\phi}} \end{Bmatrix} + \begin{bmatrix} \mathbf{K}_{uu} & \mathbf{K}_{u\phi} \\ \mathbf{K}_{\phi u} & \mathbf{K}_{\phi\phi} \end{bmatrix} \begin{Bmatrix} \mathbf{d} \\ \boldsymbol{\phi} \end{Bmatrix} = \begin{Bmatrix} \mathbf{F}_{\text{ext}}^{\text{mec}}(t) \\ \mathbf{F}^{(A)}(t) \end{Bmatrix} \quad (14)$$

where $\mathbf{F}_{\text{ext}}^{\text{mec}}(t)$ is the external excitation, and $\mathbf{F}^{(A)}(t)$ is the equivalent force of the actuator.

3 The state variable approach

Since the externally applied electric charge at the sensors is zero, the electric potential vector can be separated into a sensor component $\boldsymbol{\phi}^{(S)}$ and an actuator component $\boldsymbol{\phi}^{(A)}$, and then Eq.(14) can be transformed as (Simoes et al., 2004)

$$\begin{aligned} & \begin{bmatrix} \mathbf{M}_{uu} & \mathbf{0} & \mathbf{0} \\ \mathbf{0} & \mathbf{0} & \mathbf{0} \\ \mathbf{0} & \mathbf{0} & \mathbf{0} \end{bmatrix} \begin{Bmatrix} \ddot{\mathbf{d}} \\ \ddot{\boldsymbol{\phi}}^{(A)} \\ \ddot{\boldsymbol{\phi}}^{(S)} \end{Bmatrix} + \\ & \begin{bmatrix} \mathbf{K}_{uu} & \mathbf{K}_{u\phi}^{(A)} & \mathbf{K}_{u\phi}^{(S)} \\ \mathbf{K}_{\phi u}^{(A)} & \mathbf{K}_{\phi\phi}^{(A)} & \mathbf{0} \\ \mathbf{K}_{\phi u}^{(S)} & \mathbf{0} & \mathbf{K}_{\phi\phi}^{(S)} \end{bmatrix} \begin{Bmatrix} \mathbf{d} \\ \boldsymbol{\phi}^{(A)} \\ \boldsymbol{\phi}^{(S)} \end{Bmatrix} = \begin{Bmatrix} \mathbf{F}_{\text{ext}}^{\text{mec}}(t) \\ \mathbf{Q}^{(A)}(t) \\ \mathbf{0} \end{Bmatrix} \end{aligned} \quad (15)$$

Furthermore, Eq.(15) can be written as

$$\mathbf{M} \ddot{\mathbf{q}} + \mathbf{K}_{uu} \mathbf{q} + \mathbf{K}_{u\phi}^{(S)} \boldsymbol{\phi}^{(S)} = \mathbf{F}_{\text{ext}}^{\text{mec}} - \mathbf{K}_{u\phi}^{(A)} \boldsymbol{\phi}^{(A)} \quad (16)$$

$$\mathbf{K}_{\phi u}^{(A)} \mathbf{q} + \mathbf{K}_{\phi\phi}^{(A)} \boldsymbol{\phi}^{(A)} = \mathbf{Q}^{(A)} \quad (17)$$

$$\mathbf{K}_{\phi u}^{(S)} \mathbf{q} + \mathbf{K}_{\phi\phi}^{(S)} \boldsymbol{\phi}^{(S)} = \mathbf{0} \quad (18)$$

The induced sensory electric potentials are obtained as follows from Eq.(18):

$$\boldsymbol{\phi}^{(S)} = -\mathbf{K}_{\phi\phi}^{(S)-1} \mathbf{K}_{\phi u}^{(S)} \mathbf{q} \quad (19)$$

Substituting Eq.(19) into Eq.(16), the motion equation of undamped forced vibration becomes

$$\mathbf{M} \ddot{\mathbf{q}} + \left(\mathbf{K}_{uu} - \mathbf{K}_{u\phi}^{(S)} \mathbf{K}_{\phi\phi}^{(S)-1} \mathbf{K}_{\phi u}^{(S)} \right) \mathbf{q} = \mathbf{F}_{\text{ext}}^{\text{mec}} - \mathbf{K}_{u\phi}^{(A)} \boldsymbol{\phi}^{(A)} \quad (20)$$

Considering the Rayleigh damping, we can write

$$\mathbf{M} \ddot{\mathbf{q}} + \mathbf{C}_R \dot{\mathbf{q}} + \left(\mathbf{K}_{uu} - \mathbf{K}_{u\phi}^{(S)} \mathbf{K}_{\phi\phi}^{(S)-1} \mathbf{K}_{\phi u}^{(S)} \right) \mathbf{q} = \mathbf{F}_{\text{ext}}^{\text{mec}} - \mathbf{K}_{u\phi}^{(A)} \boldsymbol{\phi}^{(A)} \quad (21)$$

It can be transferred into state space

$$\begin{cases} \dot{x} = Ax + B\phi^{(A)} + \hat{B}u \\ y = Cx \end{cases} \quad (22)$$

where $x = \begin{Bmatrix} q \\ \dot{q} \end{Bmatrix}$ is the state variable, $\hat{B} = \begin{bmatrix} 0 \\ M^{-1} \end{bmatrix}$ is the input matrix of the external excitation, $A = \begin{bmatrix} 0 & I \\ -M^{-1}(K_{uu} - K_{u\phi}^{(S)}K_{\phi\phi}^{(S)-1}K_{\phi u}^{(S)}) & -M^{-1}C_R \end{bmatrix}$ is the system matrix, $u = F_{ext}^{mec}$ is the external excitation, $y = \phi^{(S)}$ is the output of the sensors, $B = \begin{bmatrix} 0 \\ -M^{-1}K_{u\phi}^{(A)} \end{bmatrix}$ is the input matrix of the actuators, and $C = \begin{bmatrix} -K_{\phi\phi}^{(S)-1}K_{\phi u}^{(S)} & 0 \end{bmatrix}$ is the output matrix.

4 Linear quadratic regulator output feedback control

The LQR output feedback control theory (Hu *et al.*, 2005) is used to determine the control gain. The cost function is given by

$$J = \int_0^\infty (y^T Q y + \phi^{(A)T} R \phi^{(A)}) dt \quad (23)$$

where y is the same as Eq.(22), weighting matrix Q is a semi-positive definite symmetric matrix, and R is a positive definite symmetric matrix. In the design of the LQR feedback controller, the selection of matrices Q and R has a great impact on the optimal control effectiveness. For simplicity, R is often set to be a unit matrix and Q a diagonal matrix. Different control processes can be achieved by adjusting matrix Q .

Actuator voltages are assumed to be

$$\phi^{(A)} = -G_A x \quad (24)$$

where G_A is the feedback gain which satisfies

$$G_A = R^{-1} B^T P \quad (25)$$

in which P satisfies the algebraic Riccati equation (31).

$$A^T P + PA - PBR^{-1}B^T P + C^T QC = 0 \quad (26)$$

Similarly, the solution of Eq.(26) can be derived through the above-mentioned high precision direct (HPD) integration method (Zhong *et al.*, 2007). Substituting Eq.(24) and Eq.(25) into Eq.(22), the governing equations of piezoelectric composite structures in state space take the form

$$\begin{cases} \dot{x} = (A - BR^{-1}B^T P)x + \hat{B}u \\ y = Cx \end{cases} \quad (27)$$

5 LQR of piezoelectric composite structures

Dynamic characteristics and active control capabilities of composite structures with discontinuously distributed piezoelectric layers are investigated. Piezoelectric patches bounded on the top of the beam are considered as actuators, and the patches which are bounded on the bottom of the beam are considered as sensors in the following cases.

First of all, deflections of a piezoelectric composite cantilever projected to a unit voltage are given to validate the element model. Secondly, dynamic responses of a cantilever with 1/5 of the surface bounded with piezoelectric layers subjected to transient or harmonic excitations are obtained and controlled.

5.1 Validation of the piezoelectric composite element model

The first numerical simulation is applied to validate the developed piezoelectric composite element on the basis of an experiment (Tzou *et al.*, 1990). The experimental model consists of two PVDF layers bonded together, being polarized in opposite directions. Dimensions are indicated in Fig.2, and material properties are listed in Table 1.

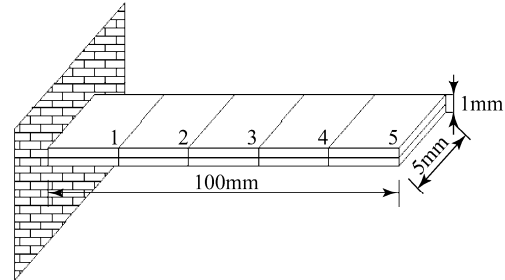


Fig.2 Finite element model of the piezoelectric composite cantilever

Table 1 Material properties of piezoelectric layers

Elastic modulus E/GPa	2.0
Density $\rho /(\text{kg}\cdot\text{m}^{-3})$	1 800
Poisson ratio μ	0.29
Electric stress constant $e_{31}/(\text{C}\cdot\text{m}^{-2})$	0.046
Electric stress constant $e_{32}/(\text{C}\cdot\text{m}^{-2})$	0.046
Electric stress constant $e_{36}/(\text{C}\cdot\text{m}^{-2})$	0
Dielectric constant $P_{33}/(\times 10^{-10} \text{ F}\cdot\text{m}^{-1})$	1.06

It can be seen from Fig.3 that the cantilever is meshed into five equal elements. The cantilever is subjected to a unit voltage between the top and bottom surfaces and the produced deflections are tabulated in Table 2. A comparison between the present numerical solution and the results in references is carried out, which shows that the developed model in this paper is feasible.

Table 2 Deflections of the cantilever produced by a unit voltage

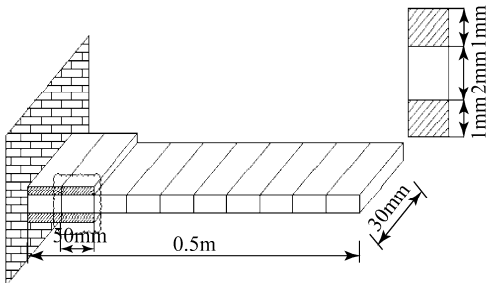
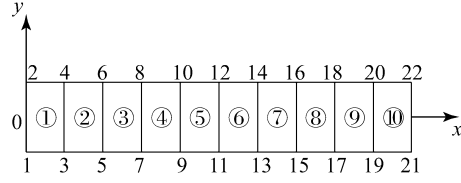
Position x/mm	Deflections / ($\times 10^{-7}$ m)				
	20.0	40.0	60.0	80.0	100.0
Theory (Tzou <i>et al.</i> , 1993)	0.138	0.552	1.24	2.21	3.45
Solid element (Tzou <i>et al.</i> , 1993)	0.124	0.508	1.16	2.10	3.30
Shell element (Tzou <i>et al.</i> , 1996)	0.132	0.528	1.19	2.11	3.30
Analytical (Gomes <i>et al.</i> , 1997)	0.130	0.510	1.14	2.02	3.16
Present	0.127	0.507	1.14	2.03	3.17
Experiment (Tzou <i>et al.</i> , 1990)	—	—	—	—	3.15

5.2 Dynamic responses of a cantilever with distributed piezoelectric sensors and actuators subjected to a harmonic excitation

A cantilever with 1/5 surfaces bounded by piezoelectric layers in the fixed end is meshed into ten equal elements, as shown in Fig.3. Element division, node serial numbers, and element serial numbers are illustrated in Fig.4; material properties of the host structure and piezoelectric sensors/actuators are tabulated in Table 3.

Table 3 Material properties of the cantilever with discontinuously distributed piezoelectric sensors and actuators

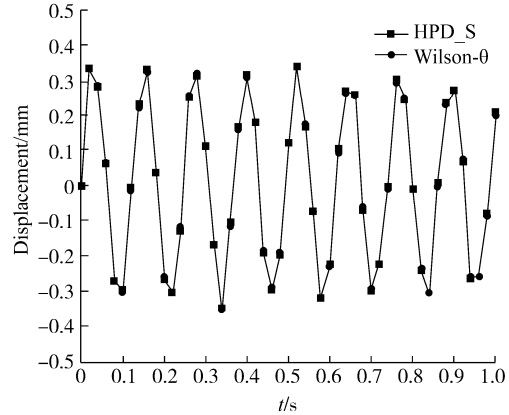
Material properties	Host structure	Piezoelectric layers
Elastic modulus E/GPa	210	63
Density $\rho/(\text{kg}\cdot\text{m}^{-3})$	7850	7500
Poisson ratio μ	0.3	0.3
Electric stress constant $e_{31}/(\text{C}\cdot\text{m}^{-2})$	/	0.046
Electric stress constant $e_{32}/(\text{C}\cdot\text{m}^{-2})$	/	0.046
Electric stress constant $e_{36}/(\text{C}\cdot\text{m}^{-2})$	/	0
Dielectric constant $P_{33}/(\times 10^{-10} \text{ F}\cdot\text{m}^{-1})$	/	150

**Fig.3 Sketch of the cantilever with 1/5 surfaces bounded with piezoelectric layers****Fig.4 Element division, node serial numbers and element serial numbers**

Based on a sub-space iteration method, the first four natural frequencies of the cantilever are 8.12, 46.19, 119.29, and 222.14 Hz.

The cantilever is subjected to an external load $F = 0.2\sin 188.4t$ (N) (at the free end. A time step $\Delta t = 1$ ms is adopted for the HPD_S (simple harmonic) method, and the Wilson- θ method as well as Rayleigh damping is considered, with coefficients of $\alpha = 3$ and $\beta = 1 \times 10^{-4}$.

Responses of the free end due to the mechanical load versus time are shown in Fig.5. The results obtained by the two methods are in a good agreement.

**Fig.5 Tip displacement response of the cantilever in time domain by the two methods**

5.3 Dynamic responses of a cantilever with distributed piezoelectric sensors and actuators subjected to an impulse excitation

An impulse excitation $F=0.2$ N is applied at the free end of the same cantilever for 1 ms. Responses of the free end due to the transient mechanical load, with a time step $\Delta t = 1$ ms being adopted for the HPD method, versus time and frequency are shown in Figs.6 and 7, respectively. The tip displacement responses of the cantilever subjected to an impulse load at the free end consists of the first four modes, among which the first mode is predominant.

5.4 LQR control of a cantilever with distributed piezoelectric sensors and actuators subjected to an impulse excitation

An impulse excitation $F=0.2$ N is applied on the free end of the same cantilever for 1 ms. A time step $\Delta t = 1$ ms is adopted for the HPD method, and Rayleigh damping is

considered with coefficients $\alpha=3$ and $\beta=1\times 10^{-4}$.

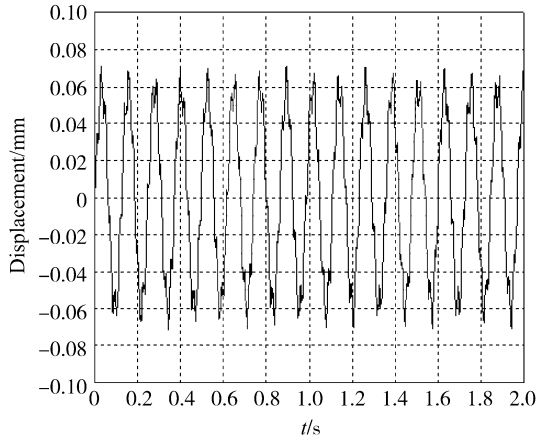


Fig.6 Tip displacement response of the cantilever without damping in time domain

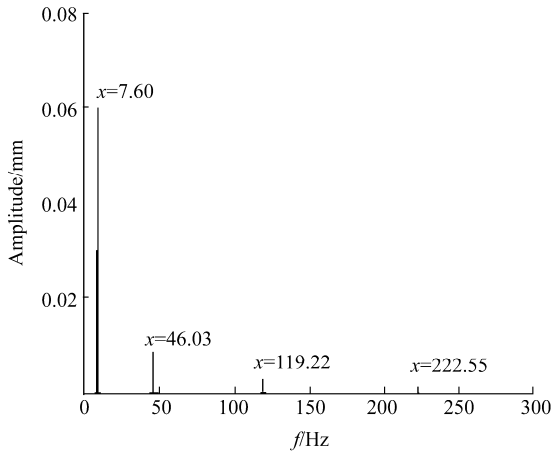
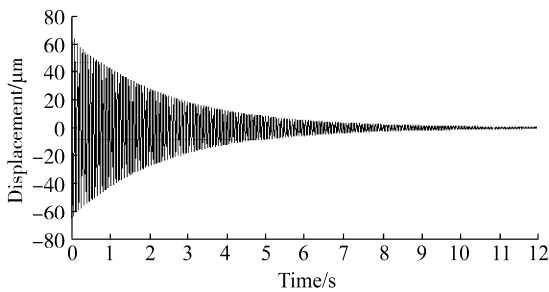
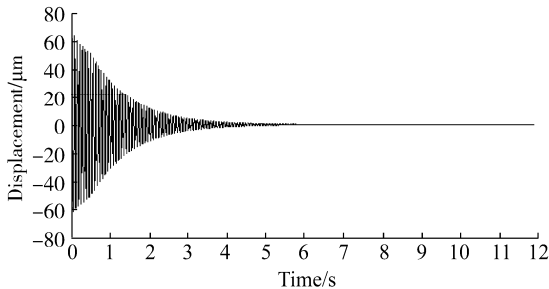


Fig.7 Tip displacement response of the cantilever without damping in frequency domain

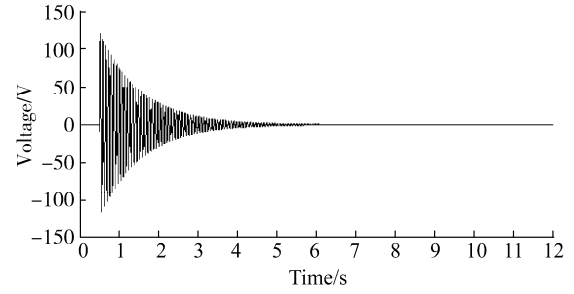


(a) Tip displacements of the cantilever without control

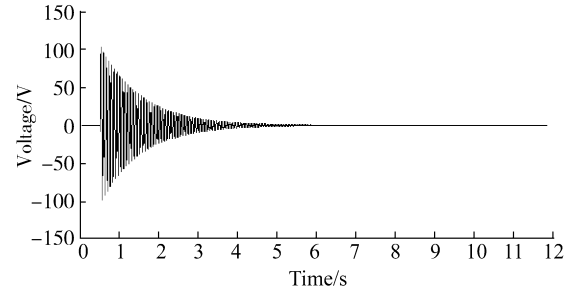


(b) Tip displacements of the cantilever with optimal control when $Q=10^{10}$

Fig.8 Tip displacements of the cantilever



(a) Voltages actuator 1 when $Q=10^{10}$



(b) Voltages actuator 2 when $Q=10^{10}$

Fig.9 Voltages Actuator1 and 2 when $Q=10^{10}$

Tip displacement responses versus time of the cantilever, in which LQR output feedback control ($Q=10^{10}$) is employed, are shown in Fig.8. Control voltages of actuators 1 and 2 are illustrated in Fig.9.

It can be seen that the amplitude of tip displacement responses attenuates rapidly after starting control at 0.5 s, reaching an equilibrium position at around 8 s. Control voltages of actuator 1 and 2 decay with the vibration attenuation.

5.5 LQR control of a cantilever with distributed piezoelectric sensors and actuators subjected to a harmonic excitation

The same cantilever is subjected to an external load $F=0.2\sin 2\pi\omega t$ (N) at the free end. Time steps $\Delta t=0.5$ ms and 0.2 ms are adopted for $\omega=500$ Hz and 1000 Hz, respectively, and Rayleigh damping is considered with coefficients $\alpha=3$ and $\beta=1\times 10^{-4}$. The effectiveness of control starting at 0.5 s and using LQR output feedback control with diagonal elements Q of the weighting matrix, Q being 10^{10} , 10^{11} , and 10^{12} , is shown in Figs.10–15 respectively.

When $\omega=1\ 000$ Hz, $\Delta t=0.2$ ms, $Q=10^{10}$; $\omega=1\ 000$ Hz, $\Delta t=0.2$ ms, $Q=10^{11}$ and $\omega=1\ 000$ Hz, $\Delta t=0.2$ ms, $Q=10^{12}$, the results of the tip displacements and voltages of actuator 1 display similar trend as shown in Figs.10–15, but the attenuation of the vibration amplitudes accelerates and actuator voltages increase while increasing the weighting matrix Q .

5.5.1 $\omega=500$ Hz, $\Delta t=0.5$ ms, $Q=10^{10}$

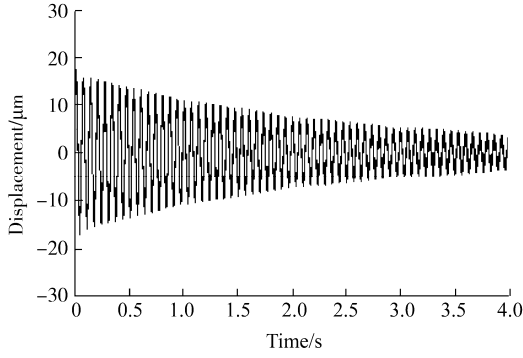


Fig.10 Controlled tip displacements of the cantilever

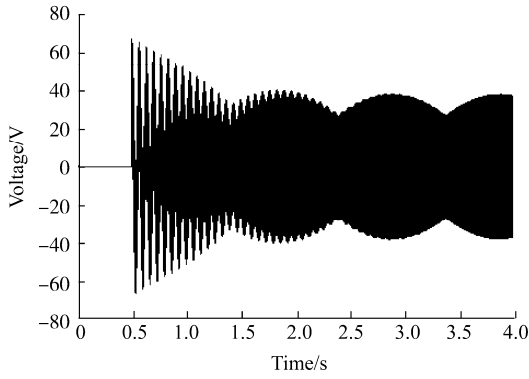


Fig.11 Voltages of actuator 1

5.5.2 $\omega=500$ Hz, $\Delta t=0.5$ ms, $Q=10^{11}$

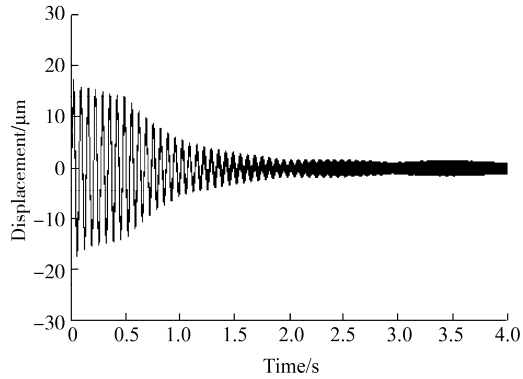


Fig.12 Controlled tip displacements of the cantilever

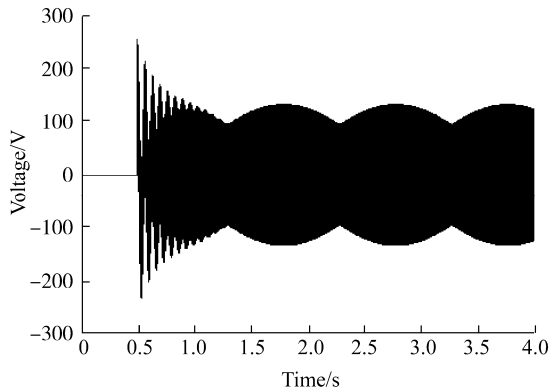


Fig.13 Voltages of actuator 1

5.5.3 $\omega=500$ Hz, $\Delta t=0.5$ ms, $Q=10^{12}$

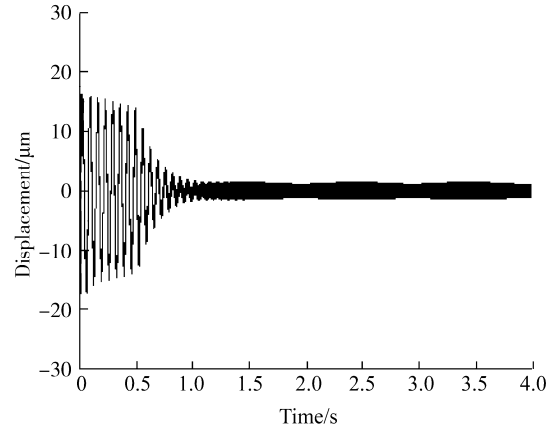


Fig.14 Controlled tip displacements of the cantilever

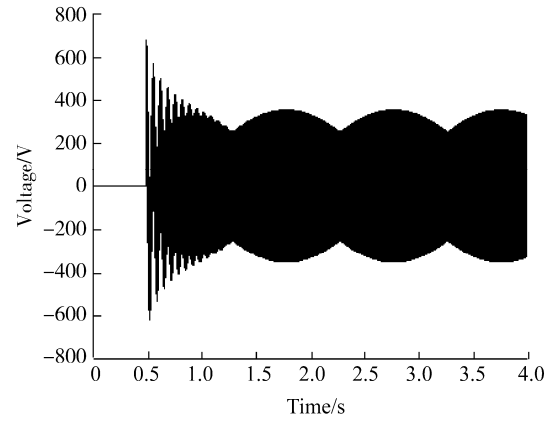


Fig.15 Voltages of actuator 1

It should be noted from Figs.10–15 and above that the LQR optimal controller designed in this paper successfully suppressed vibrations of a cantilever with discontinuously distributed piezoelectric sensors and actuators. It can be concluded as follows:

1) Amplitudes of tip displacement responses of the cantilever attenuate rapidly after starting control at 0.5 s. Voltages of actuator 1 appear to decay with the vibration attenuation.

2) When the cantilever is subjected to a certain excitation, increasing weighting matrix Q in a certain range can accelerate attenuation of the vibration amplitudes, while amplitudes of steady state vibration decay. Meanwhile, the necessary corresponding control voltages are higher. It should be noted that Q increases within the limitation of the maximum allowable voltage of the PZT used.

3) Control effectiveness with the same weighting matrix seems to be the same when the cantilever is subjected to external loads with different frequencies; however, actuator voltages increase with the increasing of excitation frequency in a certain range.

6 Conclusions

The 4-node quadrilateral piezoelectric composite element based on Mindlin first-order shear deformation theory can be used to accurately simulate electromechanical behavior of piezoelectric composite structures. The LQR output feedback controller designed in state space can suppress vibrations of a cantilever with distributed piezoelectric sensors and actuators effectively. In this paper, the corresponding FORTRAN computer programs were programmed to efficiently carry out this process. Furthermore, the high precise direct (HPD) integration method was proven to be an effective method for solving dynamic response. Selection of weighting matrices in the cost function of optimal control can influence the control effectiveness and the required energy. Assuming \mathbf{R} is a unit matrix and a larger \mathbf{Q} is selected within the limitation state, a better control effectiveness can be achieved, and more energy is needed simultaneously. The application of piezoelectric composite structures in AVC of ship structures was proven to be feasible through the vibration control of a cantilever with distributed sensors and actuators.

References

- Crawley EF, de Luis J (1986). Use of piezoelectric actuators as element of intelligent structures. *AIAA/ASME/ASCE/AHS 27th Structures, Structural Dynamics and Materials Conference*, San Antonio, Paper 86-0878.
- Gomes M (1997). *Modelling and optimization of electromechanical adaptive structures*. Master thesis, Instituto Superior Tecnico, Technical University of Lisbon, Portugal. (in Portuguese)
- Jiang Jianping, Li Dongxu (2007). A new finite element model for piezothermoelastic composite beam. *Journal of Sound and Vibration*, **306**(3-5), 849-864.
- Merek P (2008). Piezoelectric control of composite plate vibration: Effect of electric potential distribution. *Computers and Structures*. **86**(9), 948-954.
- Moita JMS, Correia IFP, Soares CMM, Soares CAM (2004). Active control of adaptive laminated structures with bonded piezoelectric sensors and actuators. *Computers and Structures*, **82**(17-19), 1349-1358.
- Narayanan S, Balamurugan V (2003). Finite element modeling of piezolaminated smart structures for active vibration control with distributed sensors and actuators. *Journal of Sound and Vibration*, **262**(3), 529-562.
- Ray MC, Bhattacharyya R, Samanta B (1993). Exact solutions for static analysis of intelligent structures. *AIAA Journal*, **31**(9), 1684-1691.
- Samanta B, Ray MC, Bhattacharyya R (1996) Finite element model for active control of intelligent structure. *AIAA Journal*, **34**(9), 1885-1893.
- Song G, Sethi V, Li H-N (2006). Vibration control of civil structures using piezoceramic smart materials: a review. *Engineering Structures*, **28**(11), 1513-1524.
- Sung Yi, Shih Fu Ling, Ming Ying (2000). Large deformation finite element analyses of composite structures integrated with piezoelectric sensors and actuators. *Finite Elements in Analysis and Design*, **35**(1), 1-15.
- Tiersten HF (1969). *Linear piezoelectric plate vibrations*. Plenum Press, New York.
- Tzou HS (1993). *Piezoelectric shells: distributed sensing and control of continua*. Kluwer Academic Publishers, Netherlands.
- Tzou HS, Teng CI (1990). Distributed piezoelectric sensor/ actuator design for dynamic measurement/ control of distributed parameter systems: a piezoelectric finite element approach. *Journal of Sound and Vibration*, **138**(1), 17-34.
- Tzou HS, Ye R (1996). Analysis of piezoelectric structures with laminated piezoelectric triangle shell element. *AIAA Journal*, **34**(1), 110-115.
- Zhang Yahui, Lin Jiahao (2007). *Fundamentals of structural dynamics*. Dalian University of Technology Press, Dalian. 5-55.
- Zhong Wanxie (1993). *Computational structural mechanics and optimal control*. Dalian University of Technology Press, Dalian.
- Zhong Wanxie, Wu Zhigang, Tan Shujun (2007). *State space control theory and computation*. Science Press, Beijing. 135-138.



Feng Chen was born in 1986. She is a master's degree candidate at Dalian University of Technology. Her research interests are ship vibration and noise control.



Ming Hong was born in 1959. He is a professor at the School of Naval Architecture, Dalian University of Technology. His research interests include ship vibration analysis, control, and experimentation as well as acoustic transmission in multi-media. He is a senior member of China Shipbuilding Institute and a member of the Ship mechanics Committee.